Armatur volume 7 nomor 2 (2026)
ISSN (cetak): 2722-080X, ISSN (online): 2722-0796

Contents list available at Sinta

ARMATUR

: Artikel Teknik Mesin & Manufaktur

Journal homepage: https://scholar.ummetro.ac.id/index.php/armatur

Structural Integrity Assessment and Remaining Fatigue Life Estimation of a Rotary Dryer Shell Using Finite Element and Fracture Mechanics Approaches

Ichsan Al Islami[1], Achmad Syaifudin[2*]

[1]Master Program in Mechanical Engineering, Department of Mechanical Engineering, Faculty of Industrial Technology and Systems Engineering, Institut Teknologi Sepuluh Nopember, Surabaya 60111, Indonesia

[2]Department of Mechanical Engineering, Faculty of Industrial Technology and Systems Engineering, Institut Teknologi Sepuluh Nopember, Surabaya 60111, Indonesia

ARTICLE INFO

Keywords:
Rotary dryer
Finite element analysis
Fracture mechanics
Fatigue crack propagation
Remaining fatigue life

ABSTRACT

Rotary dryers are widely used in fertilizer, mineral processing, and chemical industries under cyclic thermo-mechanical loading, making their shells susceptible to fatigue cracking and structural degradation during long-term service. This study evaluates the structural integrity and remaining fatigue life of a rotary dryer shell using an integrated finite element analysis (FEA) and fracture mechanics approach. A global–local finite element model was developed in ANSYS Mechanical to identify critical stress concentration regions, while submodeling was employed to improve local stress evaluation. Semi-elliptical surface cracks were introduced, and the Mode-I Stress Intensity Factor (KI) was determined using the Contour Integral method. Fatigue crack propagation and remaining fatigue life were predicted using Paris Law. The global analysis produced a maximum von Mises stress of 234.13 MPa, whereas the submodel predicted a localized stress of 874.71 MPa at the shell–riding ring welded joint. The calculated KI ranged from 203.61 to 275.72 MPa√mm, with fatigue crack growth rates between 2.67 × 10^{-9} and 6.63 × 10^{-9} m/cycle. The predicted remaining fatigue life was approximately 1.0 × 10^{7} loading cycles, equivalent to 39,682 operating hours (4.53 years). The proposed framework provides an effective basis for structural integrity assessment and

**Corresponding author*: syaifudin@its.ac.id
DOI: https://doi.org/10.24127/armatur.v7i2.12059
Received 18 June 2026; Received in revised form 24 July 2026; Accepted 29 Juny 2026
Available online September 2026

condition-based maintenance planning of rotary dryer shells.

Introduction

The rotary dryer is one of the primary pieces of equipment widely used in the fertilizer, mineral processing, chemical, and metallurgical industries for continuous material drying processes. It is capable of handling large production capacities with high operational efficiency [1],[4]. During operation, the rotary dryer shell is subjected to a combination of mechanical and thermal loads arising from its self-weight, material load, operating temperature, and interactions with the support system, including the riding ring and support rollers. These combined loading conditions produce complex stress distributions and may lead to stress concentration at critical locations [5],[7].

Continuous rotation subjects the rotary dryer shell to cyclic loading, which can initiate cracks in critical regions, particularly around welded joints and the riding ring. Once initiated, these cracks may propagate through fatigue crack growth mechanisms, ultimately reducing the structural integrity of the shell and increasing the risk of equipment failure [8],[10]. Therefore, structural condition assessment and remaining fatigue life prediction are essential for ensuring operational reliability and supporting effective maintenance planning.

Advances in numerical methods have enabled comprehensive structural behavior analysis through Finite Element Analysis (FEA). This method has been widely employed to evaluate stress distribution and deformation in structures with complex geometries and loading conditions [11],[14]. For large-scale structures such as rotary dryers, the submodeling technique can be applied to improve the accuracy of local stress evaluation in critical regions that cannot be represented in sufficient detail by a global model [15]. Furthermore, fracture mechanics approaches based on the Stress Intensity Factor (SIF) and Paris' Law enable quantitative prediction of fatigue crack propagation and estimation of the remaining fatigue life of structural components [16],[17], [21],[23].

Several previous studies have investigated the thermal and mechanical responses of rotary kilns and rotary dryers using numerical approaches [5],[6],[23]. Although previous studies have extensively investigated the thermal behavior, stress distribution, and structural response of rotary kilns and rotary dryers using numerical approaches, most of them evaluate these aspects separately. An integrated structural integrity assessment that combines global finite element analysis, local submodeling, fracture mechanics, and fatigue crack propagation analysis for predicting the remaining fatigue life of rotary dryer shells is still limited. Consequently, a comprehensive framework capable of identifying critical fatigue locations and estimating structural remaining fatigue life under cyclic operating conditions has not yet been sufficiently established.

Accordingly, this study addresses four research questions concerning the critical stress location, the effectiveness of the global–local finite element approach, the Mode-I Stress Intensity Factor and fatigue crack propagation characteristics, and the predicted remaining fatigue life under the specified operating conditions.

The novelty of this work lies in the integration of global finite element analysis, local submodeling, contour-integral-based Stress Intensity Factor evaluation, and Paris Law fatigue crack propagation into a unified framework for structural integrity assessment and remaining fatigue life prediction of rotary dryer shells. Unlike previous studies that primarily focused on stress analysis or thermal behavior, the proposed framework provides a comprehensive methodology for identifying critical locations, evaluating crack propagation behavior, and estimating the remaining fatigue life to support condition-based maintenance planning.

Research Methodology

The research commenced with the collection of technical data of the rotary dryer, followed by the development of a three-dimensional (3D) model using computer-aided design (CAD) software. The model was subsequently analyzed using the Finite Element Analysis (FEA) method to determine the deformation and stress distributions under operational loading conditions. The location exhibiting the maximum stress was identified as the critical region and further investigated using the submodeling technique. A semi-elliptical surface crack was then introduced into the critical region and evaluated using the Contour Integral method to determine the Mode-I Stress Intensity Factor (K_I). The calculated K_I values were employed as input parameters for fatigue crack growth analysis based on Paris' Law. Finally, the remaining fatigue life was estimated from the number of crack propagation cycles and converted into actual operating time based on the rotary dryer rotational speed of 4.2 rpm.

1. Research Flowchart

The research began with collecting the rotary dryer data, including geometry, operating conditions, and material properties, to develop the CAD model and define the material properties. A global finite element analysis was then conducted together with a mesh convergence study to ensure numerical accuracy. Static structural analysis was subsequently performed to obtain the stress and deformation distributions and to identify the critical region.

The identified critical region was further investigated using the submodeling technique combined with a local mesh convergence study and semi-elliptical surface crack modeling. Subsequently, fracture mechanics analysis was carried out to determine the Stress Intensity Factor (SIF) using the Contour Integral method.

The obtained SIF values were employed in fatigue crack growth analysis based on Paris' Law to predict the crack propagation rate. Finally, the remaining fatigue life was estimated from the number of loading cycles required for the crack to reach its critical size.

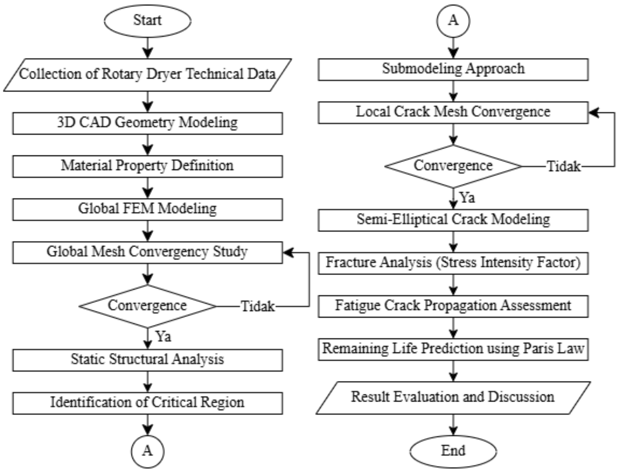

Figure 1. Research flowchart

2. Research object

The object of this study was the shell of a rotary dryer used in the fertilizer industry. The rotary dryer shell is a horizontal cylindrical structure supported by a riding ring and roller system and operates continuously during the material drying process. The shell material was ASTM A283 Grade C steel, whose mechanical properties are presented in Table 1.

Table 1. Mechanical properties of ASTM A283 Grade C steel

Material Property	Symbol	Value	Unit
Density	ρ	7800	kg/m^3
Modulus Young	E	190	GPa
Poisson's Ratio	ν	0.29	-
Yield Strength	σ_Y	205	MPa
Ultimate Tensile Strength	σ_u	380	MPa
Thermal Expansion	α	12×10^{-6}	1/°C
Thermal Conductivity	k	45	W/m·K
Specific Heat	Cp	470	J/kg·K

The geometry was developed based on the actual dimensions of the rotary dryer used in the production facility. The investigation focused on the welded joint surrounding the riding ring, where preliminary inspection and initial analyses indicated the presence of significant stress concentration.

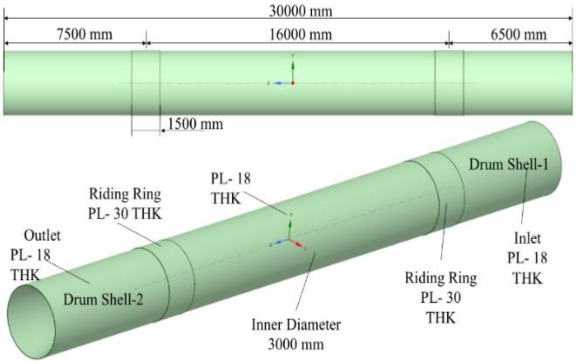

Figure 2. Geometry of the rotary dryer shell

3. Global Finite Element Modeling

Structural analysis was performed using ANSYS Mechanical to determine the deformation and stress distributions of the rotary dryer shell. FEA method has been widely employed to evaluate structural responses under complex geometrical configurations and loading conditions [11]–[13].

The model was discretized using three-dimensional solid elements, and a mesh convergence study was conducted to ensure that the simulation results were independent of mesh size. This procedure is an essential step in numerical analysis to guarantee the accuracy and stability of the simulation results [22], [23].

The global structural model was analyzed under operating loading conditions representing the actual service environment of the rotary dryer. The applied loads consisted of gravitational loading (9.81 m/s²), shell self-weight, distributed material load acting along the inner shell surface, and a uniform thermal load corresponding to the operating temperature of 90 °C. The support system was modeled using frictionless supports at the riding ring locations, allowing free circumferential movement while restricting radial displacement. Bonded contact conditions were assigned between all welded structural components to represent fully welded connections without relative sliding or separation. These boundary conditions were selected to realistically simulate the structural response of the rotary dryer during continuous operation. The applied boundary conditions and the global finite element mesh are presented in Figures 3 and 4, respectively.

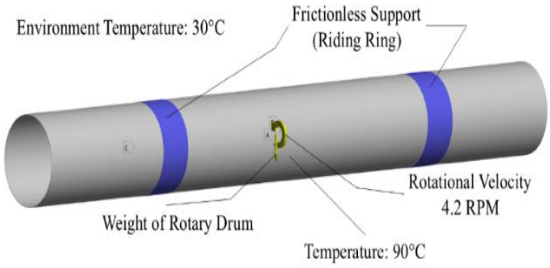

Figure 3. Boundary conditions of the global model

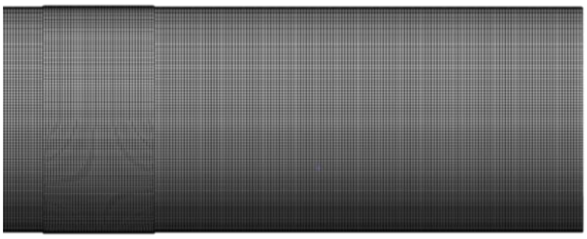

Figure 4. Global finite element mesh

Mesh quality was evaluated using the aspect ratio and skewness parameters, as summarized in Table 2. A mesh convergence study was subsequently conducted using several mesh sizes to obtain numerically stable solutions.

Table 2. Mesh quality parameters

Mesh (mm)	Elements	*Aspect Ratio Avg.*	*Aspect Ratio Max.*	*Skewness Avg.*	*Skewness Max.*
100	60000	10.91	147.61	0.53	0.99
50	184632	4.20	9.01	0.45	0.92
40	300364	3.73	7.41	0.38	0.89
35	418416	3.42	5.84	0.25	0.85
25	682104	2.13	4.29	0.27	0.76

The structural convergence results are presented in Table 3 and Figure 5. Based on these results, a global mesh size of 40 mm was selected because it provided negligible changes in stress and deformation compared with finer meshes while maintaining a balance between computational accuracy and efficiency.

Table 3. Structural convergence results

Mesh (mm)	*Max. Stress* (MPa)	*Error* (%)	*Max. Deformation* (mm)	*Error* (%)
100	213.51	-	11.259	-
50	238.17	10.35	11.256	0.03
40	234.14	1.72	11.256	0.00
35	245.86	4.77	11.255	0.01
25	251.6	2.28	11.255	0.00

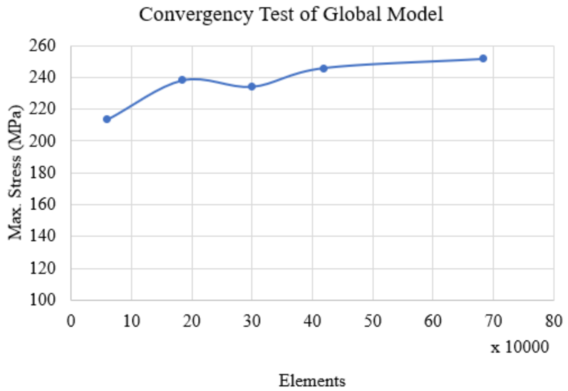

Figure 5. Global mesh convergence study

Static structural analysis was then performed to determine the total deformation and equivalent (von Mises) stress distributions throughout the structure. The global analysis results were used to identify the region with the highest stress concentration for subsequent local analysis using the submodeling technique [15].

The global finite element analysis was performed using the Static Structural module in ANSYS Mechanical with Program Controlled solver settings. Geometric nonlinearity was included by enabling the Large Deflection option. Weak springs were activated to enhance numerical stability and suppress rigid-body motion during the solution process, whereas inertia relief and quasi-static solution options were disabled because the structural response was evaluated under static operating conditions.

4. Submodel Analysis

The region exhibiting the maximum stress obtained from the global analysis was further investigated using the submodeling technique to improve the accuracy of the local stress evaluation [14]. The displacement field obtained from the solved global model was imported to the cut boundaries of the local model through the ANSYS submodeling technique, allowing the local stress distribution within the critical region to be evaluated with higher spatial resolution.

The relationship between the global model and the submodel is illustrated in Figure 6, while the finite element mesh of the local model is presented in Figure 7.

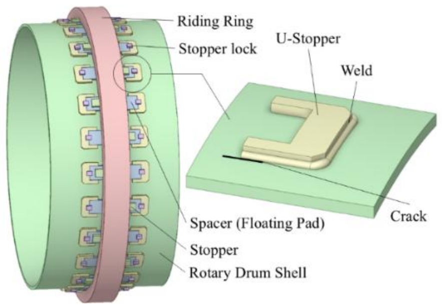

Figure 6. Relationship between the global model and the submodel

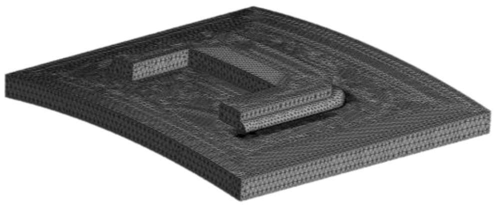
Figure 7. Mesh of the submodel

The submodel analysis results were used to determine the crack initiation location for the subsequent fracture mechanics analysis.

The local submodel was analyzed using the Static Structural module with the solver configuration set to Program Controlled. Displacement boundary conditions were imported from the global model through the submodeling technique in ANSYS Mechanical, ensuring compatibility of the displacement field at the cut boundaries, as recommended in the global–local finite element submodeling approach [14]. Since the analysis focused on a localized region surrounding the crack and inherited the global structural response, large deformation analysis and weak springs were disabled to improve computational efficiency without compromising the accuracy of the local stress field.

To verify the consistency of the displacement transfer, the total deformation predicted by the local submodel was compared with the deformation range obtained from the corresponding region of the global model. The local submodel exhibited a total deformation ranging from 5.08 to 5.51 mm, which remained within the deformation range of 4.89–6.30 mm predicted by the global model. Although the global and local models differ in geometric extent, this agreement indicates that the interpolated displacement field successfully preserved the overall structural response while enabling a more detailed evaluation of the local stress concentration.

5. Crack Modeling and Fracture Mechanics Analysis

A semi-elliptical surface crack was introduced at the location of maximum stress obtained from the submodel analysis to represent surface cracks generated by cyclic loading [15], [16]. Four crack length variations were investigated to evaluate the influence of crack growth on the K_I. The major crack length (c) was varied as 10, 20, 40, and 60 mm, while the corresponding minor crack depth (a) was proportionally assigned as 1–4 mm.

Table 4. Crack length variations

Crack Variation	*Major crack* (c) (mm)	*Minor Crack* (a) (mm)
Crack 1	10	1
Crack 2	20	2
Crack 3	40	3
Crack 4	60	4

In this study, c represents the surface crack length, whereas a denotes the crack depth propagating through the material thickness.

A local mesh convergence study was subsequently performed to ensure the accuracy of the numerical results near the crack tip. A local mesh convergence study was performed to ensure the accuracy of the stress and KI calculations around the crack tip. The convergence results are summarized in Table 5.

Table 5. Local crack mesh convergence results

Submodel Mesh (mm)	Local Crack Mesh (mm)	Elements	Max. Stress (MPa)	Error (%)	K_I (MPa √mm)	Error (%)
8	2.0	42060	894.31	-	211.04	-
6	1.5	73672	893.60	0.08	209.14	0.91
4	1.0	156873	868.52	2.89	203.06	2.99
4	0.75	175210	874.70	0.71	204.15	0.53
4	0.5	216416	871.46	0.37	203.61	0.27

Based on the convergence study, a 4 mm submodel mesh combined with a 0.75 mm local crack mesh was selected because it produced stable results with a maximum stress of 874.70 MPa and a K_I of 204.15 MPa√mm, while exhibiting only negligible differences compared with finer meshes. This mesh configuration provided an appropriate balance between computational efficiency and numerical accuracy.

The crack geometry and refined crack-tip mesh are presented in Figure 8.

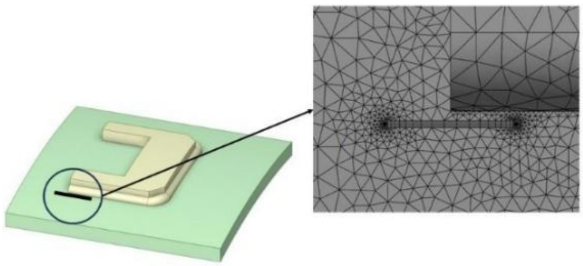

Figure 8. Semi-elliptical surface crack geometry and refined crack-tip mesh

The KI distribution along the crack front and the corresponding mesh convergence results are presented in Figures 9 and 10.

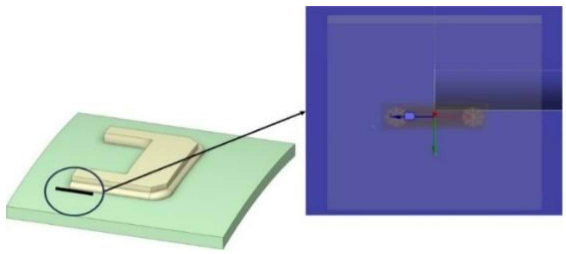

Figure 9. K_I distribution along the crack front

Figure 9 shows that the maximum KI occurs near the deepest point of the semi-elliptical crack front, whereas lower KI values are observed near the free surface. This distribution indicates that crack propagation tends to be more pronounced at the deepest crack region, which is consistent with the stress concentration characteristics of semi-elliptical surface cracks.

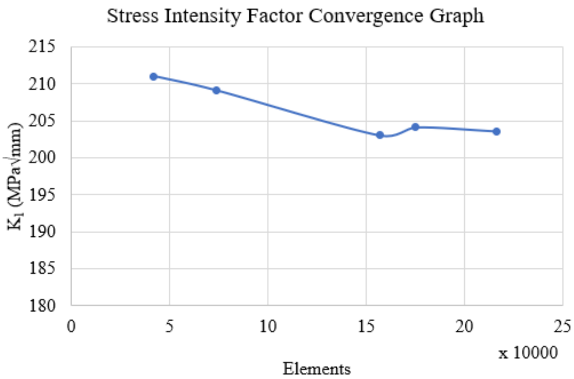

Figure 10. K_I convergence study

Figure 10 demonstrates that the calculated KI converges as the local crack mesh is refined. The variation between the last two mesh refinements is negligible, indicating mesh-independent results.

The fracture mechanics analysis was performed under the assumptions of Linear Elastic Fracture Mechanics (LEFM). The shell material was assumed to be homogeneous, isotropic, and linearly elastic throughout the analysis. Crack propagation was assumed to occur under K_I loading, and plastic deformation at the crack tip was considered negligible. These assumptions are consistent with the applicability requirements of the Contour Integral method and Paris Law adopted in this study.

6. Fatigue Crack Growth Analysis

Fatigue crack propagation was predicted using Paris' Law, which describes the relationship between crack growth rate and the stress intensity factor range (ΔK) [21].

$$\frac{da}{dN} = C(\Delta K)^m \quad (1)$$

where:

da/dN = crack growth rate (mm/cycle)

C = material constant (2×10^{-13})

ΔK = stress intensity factor range (MPa√m)

m = material exponent (3.0)

The material constants were adopted from fatigue crack growth data for carbon steel specified in ASTM E647 [22]. The simulated SIF values were used to determine the crack propagation rate for each crack length variation.

7. Remaining Fatigue Life Estimation

The remaining fatigue life was estimated based on the fatigue crack growth analysis using the numerical integration approach of Paris' Law [8], [21], [23]. The number of loading cycles required for crack propagation from the initial crack length to the critical crack length was calculated and subsequently converted into actual operating time.

The conversion was performed using the rotary dryer rotational speed of 4.2 rpm, assuming that one complete revolution corresponds to one loading cycle. The estimated operating time was then used to predict the remaining fatigue life of the rotary dryer shell and to provide recommendations for inspection intervals in the identified critical region.

Results and Discussion

1. Global Finite Element Analysis Results

The simulation results indicate that the maximum deformation of 11.256 mm occurred at both ends of the rotary dryer shell, as illustrated in Figure 11. The deformation pattern exhibits a typical bending behavior resulting from the distributed loading acting along the cylindrical structure [5], [6].

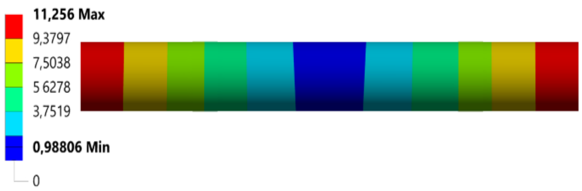

Figure 11. Total deformation distribution of the global model

The von Mises stress distribution obtained from the global finite element analysis is presented in Figure 12. The maximum equivalent stress reached 234.13 MPa and was concentrated at the junction between the shell and the riding ring, whereas the remaining shell experienced relatively lower and more uniformly distributed stresses.

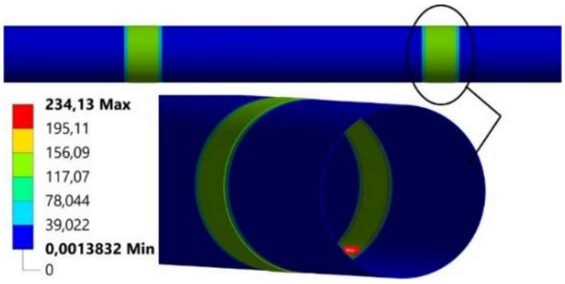

Figure 12. Von Mises stress distribution of the global model

The stress concentration at the shell–riding ring junction is attributed to the local stiffness discontinuity and geometric discontinuity, which cause load redistribution in this region [7], [24]. The maximum von Mises stress of 234.13 MPa slightly exceeds the nominal yield strength of ASTM A283 Grade C (205 MPa), corresponding to a minimum safety factor of approximately 0.88. This localized overstress is confined to the shell–riding ring welded connection, where the abrupt stiffness transition generates significant stress concentration. In the present study, the global finite element analysis was primarily intended to identify the critical location susceptible to fatigue crack initiation rather than to evaluate the onset of plastic collapse. Therefore, the identified critical region was further investigated using fracture mechanics to assess crack propagation and remaining fatigue life under the assumptions of linear elastic fracture mechanics. Based on these results, the shell–riding ring junction was identified as the most critical location and selected for further investigation using the submodeling technique to obtain a more accurate local stress distribution [15].

2. Submodel Analysis Results

Submodel analysis was performed on the critical region identified from the global analysis to obtain a more accurate representation of the local deformation and stress distributions. The simulation results showed a maximum deformation of 5.5061 mm, which was concentrated around the shell–riding ring junction, as presented in Figure 13.

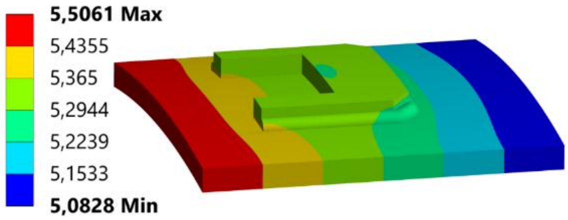

Figure 13. Deformation distribution of the submodel

The local stress distribution obtained from the submodel analysis is presented in Figure 14. The maximum stress reached 874.71 MPa, which is approximately 3.7 times higher than the maximum stress predicted by the global model (234.13 MPa).

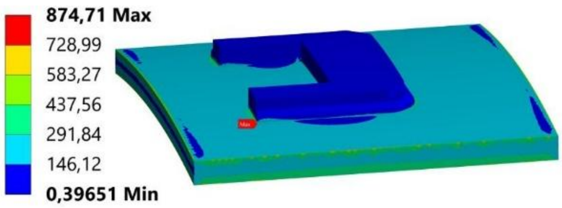

Figure 14. Stress distribution of the submodel

This significant increase demonstrates that the submodel captures the localized stress concentration at the shell–riding ring junction more accurately than the global model [14], [15]. Therefore, the location of maximum stress was selected as the crack initiation site for the subsequent fracture mechanics analysis.

Field inspection identified seven fatigue cracks located around the inlet and outlet tire regions, with measured crack lengths ranging from 60 to 420 mm. These observed damage locations correspond well with the critical stress region predicted by the finite element and submodel analyses, indicating that the numerical model successfully identified the most vulnerable structural region. Although quantitative validation of stress magnitude was not available, the qualitative agreement between the numerical prediction and field inspection supports the reliability of the proposed approach.

3. Stress Intensity Factor Analysis

The K_I was calculated using the Contour Integral method in ANSYS Mechanical for each crack length modeled at the maximum stress location identified from the submodel analysis. The calculated K_I values are summarized in Table 6.

Table 6. K_I for each crack variation

Crack Variation	K_I (MPa√mm)
Crack 1	203.61
Crack 2	260.00
Crack 3	251.14
Crack 4	275.72

The calculated K_I ranged from 203.61 to 275.72 MPa√mm. In general, increasing crack length resulted in higher stress intensity factors, indicating a greater stress concentration at the crack tip. The highest K_I value was obtained for Crack 4 (275.72 MPa√mm), while the lowest value corresponded to Crack 1 (203.61 MPa√mm). These results indicate that larger cracks possess a higher tendency for crack propagation than smaller cracks [16], [17].

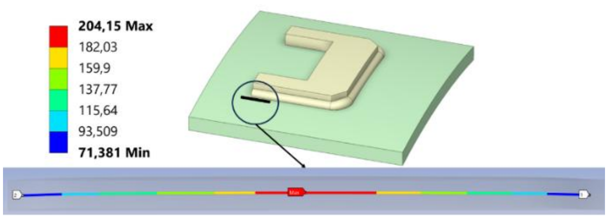

Figure 15. Local stress field around the crack tip obtained from the fracture mechanics model

Figure 15 illustrates the highly localized stress concentration around the crack tip, confirming that the crack tip experiences the highest stress intensity and therefore governs crack propagation.

The calculated K_I ranged from 203.61 to 275.72 MPa√mm. Although direct quantitative comparison with previous studies is difficult because the stress intensity factor strongly depends on crack geometry, structural dimensions, loading conditions, and boundary constraints, the increasing trend of KI with crack length observed in this study agrees well with previous investigations on welded rotary kiln shells.

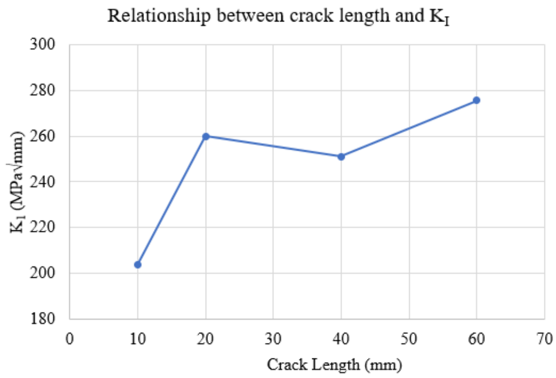

Figure 16. Relationship between initial crack length and K_I

Basri et al. [18] reported that increasing stress intensity factor accelerated fatigue crack propagation in rotary kiln shells subjected to cyclic loading, while Shen et al. [19] demonstrated that stress concentration around the shell–support connection governed the remaining fatigue life of rotary kiln structures. Similar observations have also been reported for cracked shell structures, where larger crack lengths resulted in higher stress intensity factors and faster fatigue crack growth [20].

The calculated K_I values were subsequently used as the primary input parameters for fatigue crack growth analysis and remaining fatigue life prediction of the rotary dryer shell.

4. Fatigue Crack Growth Analysis

Fatigue crack growth analysis was performed using Paris' Law to evaluate the crack propagation rate based on the ΔK obtained from the fracture mechanics analysis [21], [22]. The calculated ΔK values and crack growth rates (da/dN) are summarized in Table 7.

Table 7. Fatigue crack growth analysis results

Crack Variation	ΔK (MPa√m)	da/dN (m/cycle)
Crack 1	6.44	2.67×10^{-9}
Crack 2	8.22	5.56×10^{-9}
Crack 3	7.94	5.01×10^{-9}
Crack 4	8.72	6.63×10^{-9}

The results demonstrate that the crack growth rate generally increases with increasing crack length and ΔK. The lowest crack growth rate was obtained for the 10 mm crack, with a value of 2.67×10^{-9} m/cycle, whereas the highest rate occurred for the 60 mm crack, reaching 6.63×10^{-9} m/cycle. Although a slight decrease was observed for the 40 mm crack, the overall trend indicates that larger cracks propagate at a faster rate.

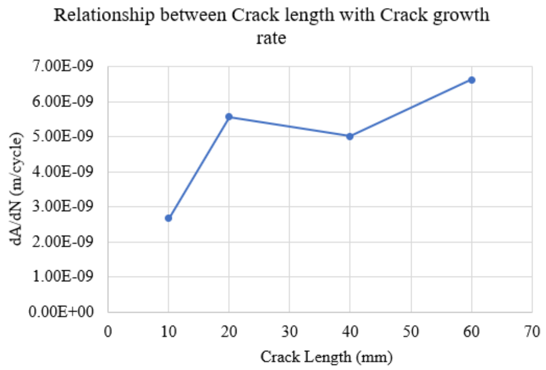

Figure 17. Relationship between crack length and crack growth rate

As illustrated in Figure 17, the fatigue crack growth rate increases progressively with increasing stress intensity factor range (ΔK). This increase in crack propagation rate is attributed to the increasing stress intensity around the crack tip, as reflected by the larger ΔK values. This behavior agrees well with Paris' Law, which predicts an exponential increase in crack growth rate with increasing ΔK [21], [23]. These findings indicate that once a crack reaches a larger size, it propagates more rapidly and may accelerate structural failure if periodic inspection and maintenance are not implemented.

5. Remaining fatigue life Estimation

The remaining fatigue life was estimated based on the fatigue crack growth analysis using the numerical integration approach of Paris' Law. The predicted crack growth curve as a function of loading cycles is presented in Figure 18.

The simulation results indicate that the crack length increases progressively as the number of loading cycles increases. Crack propagation from the initial crack length to the critical crack length is predicted to occur after approximately 1.0×10^7 loading cycles, indicating that the rotary dryer shell retains sufficient structural integrity despite the presence of crack initiation in the critical region.

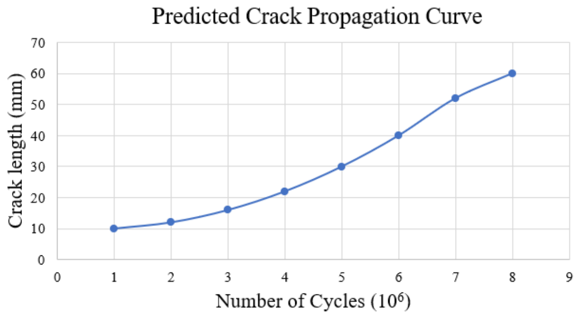

Figure 18. Predicted fatigue crack propagation and remaining fatigue life estimation

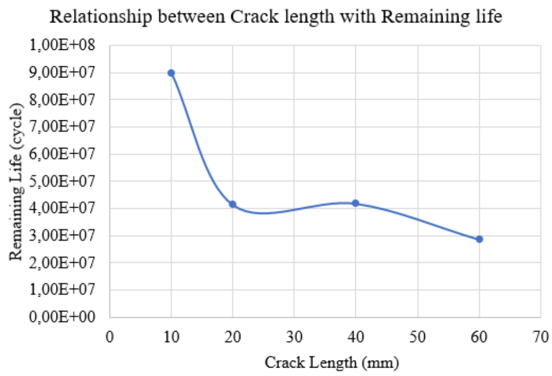

Figure 19. Relationship between crack length and remaining life

Figure 19 shows that the remaining fatigue life decreases nonlinearly as the crack length increases. Small increases in crack length at the later stage result in a significant reduction in the predicted remaining life, indicating accelerated crack propagation as failure approaches.

To provide a more practical interpretation, the predicted loading cycles were converted into actual operating time using the rotary dryer rotational speed of 4.2 rpm, assuming that one complete revolution corresponds to one loading cycle. The calculation yielded an estimated remaining fatigue life of approximately 39,682 operating hours, equivalent to 4.53 years of continuous operation.

These results demonstrate that the shell–riding ring junction has a dominant influence on the fatigue life of the structure. Although the estimated remaining fatigue life remains relatively long, continuous crack propagation may progressively reduce structural integrity if periodic inspections are not performed. Therefore, the predicted remaining fatigue life can serve as a quantitative basis for establishing inspection intervals and preventive maintenance strategies to minimize the risk of long-term structural failure [8], [23].

6. Discussion

The present study demonstrates that the rotary dryer shell primarily experiences a global bending response, with significant stress concentration occurring at the shell–riding ring junction due to geometric discontinuity and local stiffness variation. This region was consistently identified as the most critical location based on the global finite element analysis.

Comparison between the global and submodel analyses revealed that the submodel predicted substantially higher stress levels, indicating its superior capability to capture localized stress concentrations. This finding confirms the importance of employing the submodeling technique when evaluating structural integrity in critical regions where the global model cannot adequately represent local stress gradients.

The fracture mechanics analysis further showed that the K_I generally increased with increasing crack length, indicating a higher tendency for crack propagation. The subsequent Paris' Law analysis demonstrated that the fatigue crack growth rate increased with increasing ΔK, following the expected theoretical trend despite minor numerical fluctuations.

The remaining fatigue life assessment predicted that the rotary dryer shell could continue operating for approximately 1.0×10^7 loading cycles, corresponding to 4.53 years of continuous service. Nevertheless, the shell–riding ring junction remains the most critical structural region because it governs both crack initiation and subsequent crack propagation.

Overall, the results demonstrate that integrating global finite element analysis, submodeling, and fracture mechanics provides an effective framework for identifying critical regions, accurately evaluating local stress concentrations, predicting fatigue crack propagation, and estimating the remaining fatigue life of rotary dryer structures. This integrated methodology can support condition-based maintenance planning and improve the structural reliability of large rotating industrial equipment.

Conclusion

This study evaluated the structural integrity of a rotary dryer shell by integrating Finite Element Analysis (FEA), submodeling, fracture mechanics, fatigue crack growth analysis, and remaining fatigue life assessment. The global finite element analysis revealed that the maximum von Mises stress of 234.13 MPa occurred at the shell–riding ring junction, identifying this region as the most critical location due to stress concentration induced by local stiffness discontinuities. The submodel analysis predicted a significantly higher maximum stress of 874.71 MPa with a maximum deformation of 5.5061 mm, demonstrating its ability to accurately capture the local stress distribution and identify the crack initiation site. Fracture mechanics analysis showed that the K_I ranged from 203.61 to 275.72 MPa√mm, generally increasing with crack length. Furthermore, the fatigue crack growth analysis yielded a ΔK of 6.44–8.72 MPa√m and crack growth rates (da/dN) ranging from 2.67×10^{-9} to 6.63×10^{-9} m/cycle, indicating progressive crack propagation under cyclic loading conditions. Based on Paris' Law, the remaining fatigue life of the rotary dryer shell was estimated to be approximately 1.0×10^7 loading cycles corresponding to 39,682 operating hours or approximately 4.53 years of continuous operation at a rotational speed of 4.2 rpm.

The predicted remaining fatigue life provides a quantitative basis for establishing inspection intervals, implementing predictive maintenance strategies, and supporting risk-based inspection (RBI) programs for rotary dryer systems. By identifying the shell–riding ring junction as the most critical structural region, the proposed methodology enables maintenance activities to be prioritized before fatigue cracks propagate to critical dimensions, thereby improving operational reliability and reducing the risk of unexpected structural failure.

Future research should incorporate elastic–plastic fracture mechanics, residual welding stresses, thermal loading, and experimental validation to further improve the accuracy of fatigue crack growth prediction and remaining fatigue life estimation. In addition, advanced crack propagation techniques such as XFEM or adaptive remeshing may be employed to predict crack propagation paths under complex operating conditions.

Referensi

[1] A. R. Vargas, et al., "Performance evaluation of a flighted rotary dryer for lateritic ore in concurrent configuration," Heliyon, vol. 9, no. 11, 2023, doi: 10.1016/j.heliyon.2023.e21345.

[2] A. Echeeri and M. Maalmi, "Performance evaluation of a rotary dryer in both co-current and counter-current configurations," Journal of Thermal Engineering, vol. 7, Supplement 14, pp. 1945–1957, 2021, doi: 10.18186/thermal.1051277.

[3] S. Deng, Y. Yu, et al., "Energy efficiency analysis of a rotating-drum dryer using hot steel balls for converter sludge," Case Studies in Thermal Engineering, vol. 49, p. 103389, 2023, doi: 10.1016/j.csite.2023.103389.

[4] M. G. Petrescu, et al., "Estimating the lifetime of rotary dryer flights based on experimental data," Processes, vol. 12, no. 5, 2024, doi: 10.3390/pr12050993.

[5] W. D. Guillin-Estrada, et al., "Transient operation effects on the thermal and mechanical response of a large-scale rotary kiln," Results in Engineering, vol. 14, p. 100396, 2022, doi: 10.1016/j.rineng.2022.100396.

[6] K. I. Janati, "Thermo-elastic behavior study of rotary kilns for cement plants," Engineering Failure Analysis, vol. 118, p. 104896, 2020, doi: 10.1016/j.engfailanal.2020.104896.

[7] S. El Fakkoussi, et al., "Analytical and numerical analysis of the tire tightening system of a cement kiln," International Journal on Interactive Design and Manufacturing, vol. 14, no. 2, pp. 359–366, 2020, doi: 10.1007/s12008-019-00592-5.

[8] U. Zerbst, M. Madia, et al., "The impact of fracture mechanics on fatigue assessment of engineering structures," Engineering Fracture Mechanics, vol. 231, p. 107031, 2020.

[9] M. Song, et al., "Fatigue life assessment of the shell structure of purified terephthalic acid filter press," Materials, vol. 13, no. 3276, pp. 1–16, 2020.

[10] A. Burlacu, et al., E. Laudacescu, I. Ramadan, and C. Ilincă, "Numerical approach regarding the effect of the flight shape on the performance of rotary dryers from asphalt plants," Processes, vol. 10, no. 11, 2022, doi: 10.3390/pr10112339.

[11] D. Harnany, et al., "Strength consideration on car body modification for panoramic train," Jurnal Rekayasa Mesin, vol. 15, no. 1, pp. 355–366, 2024.

[12] A. R. Hakim, et al., "Finite element analysis of a new acetabular plate in the combined posterior column and posterior acetabular wall fracture model," Hip & Pelvis, vol. 37, no. 1, pp. 72–82, 2025.

[13] I. G. A. W. Ardani, et al., "Comparison of biomechanical performance of

titanium and polyaryletheretherketone miniscrews at different insertion angles: A finite element analysis," Journal of Orthodontic Science, vol. 13, no. 1, p. 13, 2024.
[14] Y. Li, et al., "Global-local finite element submodeling approach for stress evaluation of large-scale engineering structures," Engineering Structures, vol. 266, p. 114612, 2022.
[15] X. Zhu, et al., "Numerical evaluation of stress intensity factors using finite element contour integral methods," Engineering Failure Analysis, vol. 138, p. 106322, 2022.
[16] ASTM International, ASTM E399-24: Standard Test Method for Linear-Elastic Plane-Strain Fracture Toughness of Metallic Materials. West Conshohocken, PA, USA: ASTM International, 2024.
[17] T. L. Anderson, Fracture Mechanics: Fundamentals and Applications, 4th ed. Boca Raton, FL, USA: CRC Press, 2017.
[18] H. Basri, et al., "The prediction of fatigue crack growth of rotary kiln shell welded under cyclic loading," Sriwijaya international Conference on Science, Engineering, and Technology, IOP Conf. Series: Materials Science and Engineering 620, pp. 1-8, 2019, doi: 10.1088/1757-899X/620/1/012115
[19] Y. P. Shen, et al., "Fatigue propagation lifetime prediction of rotary kiln weld shell," Applied Mechanics and Materials, vol. 34-35, pp. 1724-1729, 2010.
[20] A. Carpinteri, et al., "Stress intensity factors and fatigue growth of surface cracks in notched shells and round bars: two decades of research work," Fatigue and Fracture of Engineering Materials & Structures, pp. 1-13, 2013, doi: 10.1111/ffe.12092.
[21] P. Paris and F. Erdogan, "A critical analysis of crack propagation laws," Journal of Basic Engineering, vol. 85, no. 4, pp. 528–533, 1963.
[22] ASTM International, ASTM E647-23: Standard Test Method for Measurement of Fatigue Crack Growth Rates. West Conshohocken, PA, USA: ASTM International, 2023.
[23] S. Suresh, Fatigue of Materials, 2nd ed. Cambridge, U.K.: Cambridge University Press, 1998.
[24] D. Zahradník, et al., "Investigation of inner lining loss and correlation with steel structure ovality in rotary kilns," Applied Sciences, vol. 13, no. 23, p. 12811, 2023, doi: 10.3390/app132312811.